Synthesis of potassium–sodium niobate (KNN) from NbO_2

Cerem Piskin [a], Levent Karacasulu [a], Mauro Bortolotti [b], Cekdar Vakifahmetoglu [a,*]

[a] Department of Materials Science and Engineering, Izmir Institute of Technology, 35430, Urla, Izmir, Turkey
[b] Department of Industrial Engineering, University of Trento, Via Sommarive 9, 38123, Trento, Italy

A R T I C L E   I N F O

A B S T R A C T

$K_xNa_{1-x}NbO_3$ ($0 < x < 1$) were synthesized via hydrothermal method using niobium dioxide (NbO_2) as the niobium source instead of the most common one, Nb_2O_5. Potassium-rich $K_xNa_{1-x}NbO_3$ ($x > 0.5$) was obtained from 8 M total hydroxide concentration after 6 h of reaction at 200 °C. Rietveld refinement of the XRD data revealed that all samples exhibited the secondary $NaNbO_3$ phase. However, the lowest amount (3.74 vol%) was obtained for 24 h of reaction under 10 M alkaline solution. After 3 h of reaction, dodecahedra shaped hexaniobate phase ($K_xNa_{8-x}Nb_6O_{19}.nH_2O$) was observed. Those structures were, subsequently, replaced by ~3 μm cube shaped KNN crystals, obtained under 10 M reaction in 24 h time period.

1. Introduction

Piezoelectric ceramics are the group of functional crystalline materials having various applications in pressure sensors, surface acoustic wave (SAW) devices, ultrasonic transducers and motors, transformers & actuators and so on [1,2]. Lead based, e.g., lead zirconate titanate (PZT), ceramics have been majorly used to manufacture these electronic devices due to their decent electromechanical properties [3]. Nevertheless, lead is a toxic material, and PZT ceramics possess a lead content of more than 60 wt percent [4]. Lately, governmental regulations, aiming at limiting the use of hazardous substances, have been introduced [5–7]. For this reason, it became urgent to find alternative lead free piezoelectric materials having comparable properties with that of the lead including counterparts [8].

Alkali niobate based piezoelectric ceramics, e.g., $K_xNa_{1-x}NbO_3$ (broadly abbreviated as KNN) have attracted tremendous attention with the demand of lead free piezoceramics [4,8–10]. Besides offering a relatively high Curie temperature ($T_c \cong 418$ °C), KNN ceramics pose a large piezoelectric coefficient ($d_{33} = 80$ pC/N) [11] when the composition is at the morphotropic phase boundary (MPB), i.e., $x \cong 0.5$ ($K_{0.5}Na_{0.5}NbO_3$), was achieved [5,12,13]. Electrical properties of KNN have high sensitivity to the chemical composition, thus it becomes crucial to preserve desired stoichiometry during both powder synthesis and monolith production to obtain the best possible electrical properties. While there are several challenges with the route, KNN has been mostly synthesized by the conventional solid-state method. The raw materials for solid state synthesis (generally alkali carbonates) have

hygroscopic nature causing poor purity [10,14,15]. Additionally, deviations in the stoichiometry may occur when high temperature processes, e.g., calcination and sintering are applied because uneven volatilization of alkali oxides (Na_2O and K_2O) takes place as a result of their relatively high volatility [16]. Therefore, instead of solid-state technique, wet chemical routes have been proposed for KNN powder synthesis. Among those, this paper focused on hydrothermal reaction due to the ability to synthesize high crystallinity powders at moderate temperatures [17].

In KNN powder synthesis processes, the most used niobium source is Nb_2O_5 (niobium pentoxide) [11,17–20]. On the other hand, there is NbO_2, a metastable phase with high reactivity [21] and such source has never been used as a precursor to produce KNN probably due to its higher cost compared to that of the most widely used Nb_2O_5. This study, for the first time, aims to synthesize $K_xNa_{1-x}NbO_3$ ($0 < x < 1$) powders by using NbO_2 as the niobium source via hydrothermal route.

2. Experimental procedure

NaOH (CAS#: 1310-73-2, 98–100%, Sigma Aldrich, USA), KOH (CAS#: 1310-58-3, ≥86%, Sigma Aldrich, USA), and NbO_2 (CAS#: 12034-59-2, 99.9%, Sigma Aldrich, USA) were used as is. First, an alkaline solution having the total alkaline concentration of 6, 8, and 10 M with a K^+/Na^+ ratio adjusted to 6, was prepared by dissolving NaOH and KOH in deionized (DI) water. NbO_2 was then added into the solution and stirred for 1 h to obtain a homogeneous dispersion. Due to the strong basic medium (pH ~ 14), Teflon reaction vessel was used with a filling
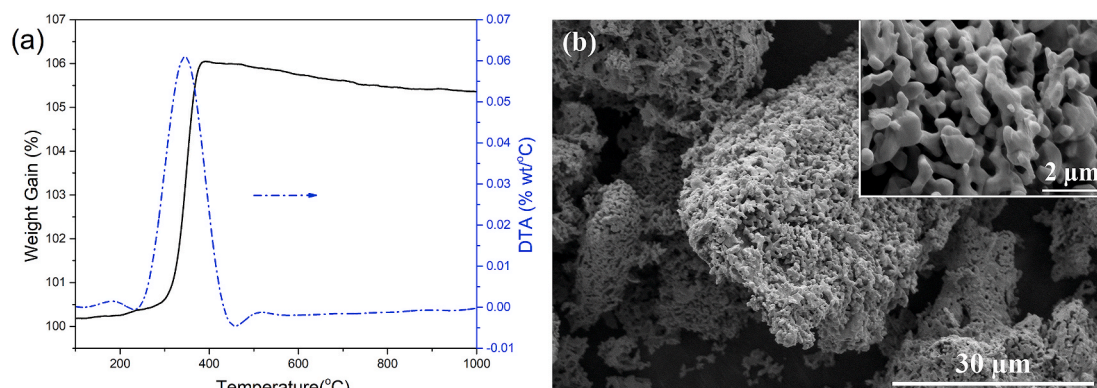
Fig. 1. (a) TGA analysis of NbO$_2$ (as received), (b) SEM images of as received NbO$_2$ powder used for the KNN synthesis, the top-right inset taken from higher magnification demonstrates the surface details.
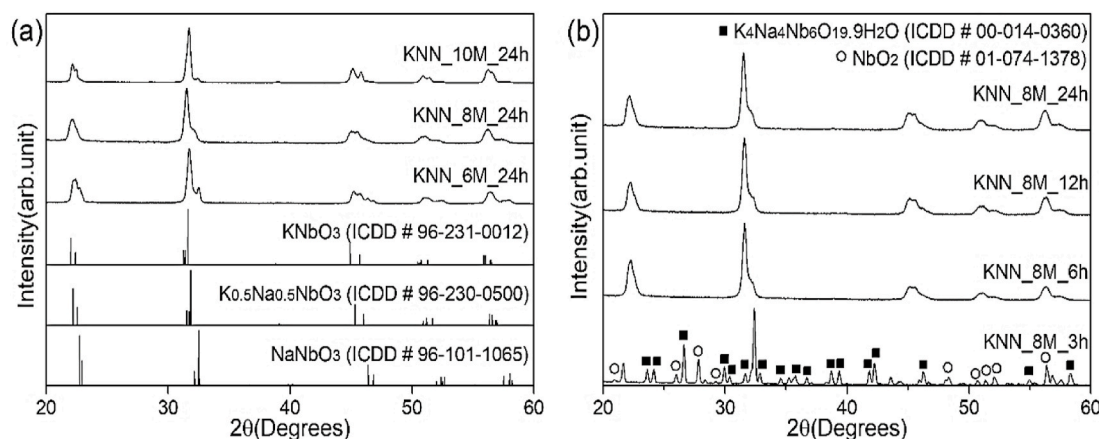

Fig. 2. Normalized X-ray diffraction patterns of; (a) ICDD data of K$_x$Na$_{1-x}$NbO$_3$ (0 ≤ x ≤ 1) and KNN powders synthesized at 200 °C by reacting alkaline solutions of total 6, 8 and 10 M total OH$^-$ concentration with NbO$_2$ for 24 h, (b) KNN powders synthesized at 200 °C by reacting the alkaline solution of total 8 M total OH$^-$ concentration with NbO$_2$ for 3, 6, 12 and 24 h.

factor of 70 vol%, sealed within a stainless-steel autoclave (Parr instruments, model 4748 A acid digestion bomb), and placed in an oven (Memmert, UN55, France) for hydrothermal reaction at 200 °C for different reaction periods. Upon reaction completion, the resultant powder was washed using DI water until pH neutrality was obtained, filtrated via vacuum filtration, and dried at room temperature (RT). The post-heat treatment was performed at 800 °C for 2 h in the air using an elevating furnace (Protherm, Ankara, Turkey).

Crystal phases of all samples were identified by an X-ray diffractometer (XRD, Panalytical X'Pert PRO, The Netherlands with a Copper anode X-Ray source [Cu$_{K\alpha}$ = 1.5406 Å at 40 kV, 30 mA]) over 20°–60° (2θ) range, besides for the Rietveld refinements, the data were collected on an Italstructures IPD3000 diffractometer equipped with a Co anode source [Co$_{K\alpha}$ = 1.7902 Å at 40 kV, 30 mA] coupled to a multilayer monochromator and Inel CPS120 detector over the 15°–110° (2θ) range with a step size of 0.03° and a counting time of 1800 s in total. The morphology of the final powders (after coating with gold) was analyzed by scanning electron microscopy (SEM, FEI Quanta 250 FEG, USA). Thermogravimetric analysis was carried out by a thermogravimetric analyzer (Pyris Diamond TG/DTA, PerkinElmer Instrument, USA) in ambient air with a heating rate of 5 °C/min to investigate the thermal stability of NbO$_2$ (as received) for the temperatures reaching up to 1200 °C. Also, the specific surface area of the as received precursor powder was determined by Gemini V (Micromeritics, Norcross, GA, USA).

3. Results and discussion

TGA analysis, given in Fig. 1(a), demonstrates ∼ 6% weight gain which is in agreement with the theoretical value [22], that starts around 200 °C and peaks at around 300 °C, caused by oxidation of NbO$_2$ to form a stable Nb$_2$O$_5$ phase. The reaction is also accompanied by a clear exothermic peak in the DTA. The morphology of the as is NbO$_2$ powder was shown in Fig. 1(b), besides the top-right inset given in the figure demonstrating the higher magnification image. As can be seen, approximately 20 μm sized aggregates are having co-continuous structures made of micron ranged small particles and interconnected large macropores [23], causing the specific surface area of the powder as 2.023 m^2/g.

XRD analyses of synthesized powders are given in Fig. 2(a&b). The ICDD data are also reported at the bottom of Fig. 2(a) to emphasize the challenges in K$_x$Na$_{1-x}$NbO$_3$ characterization by X-ray analysis; e.g., the resemblance of the patterns for three distinct niobium oxide phases. To begin with, patterns of all samples synthesized under 6, 8, and 10 M total OH$^-$ concentration, exhibit K-rich KNN phase (K$_x$Na$_{1-x}$NbO$_3$, x > 0.5). This can be determined by realizing the peak shift to lower 2θ angles compared to K$_{0.5}$Na$_{0.5}$NbO$_3$ (ICDD # 96-230-0500). Although, the shift is not more than 0.1° (2θ), it indicates significant changes in the stoichiometry. Considering the larger ionic radius of potassium (1.33 Å) in comparison with that of the sodium (0.95 Å) [24], a shift to lower 2θ angles is expected as a consequence of the enhanced interplanar distance originating from the incorporation of potassium ions into the crystal lattice [25]. Besides, another phase is identified as NaNbO$_3$ (ICDD #
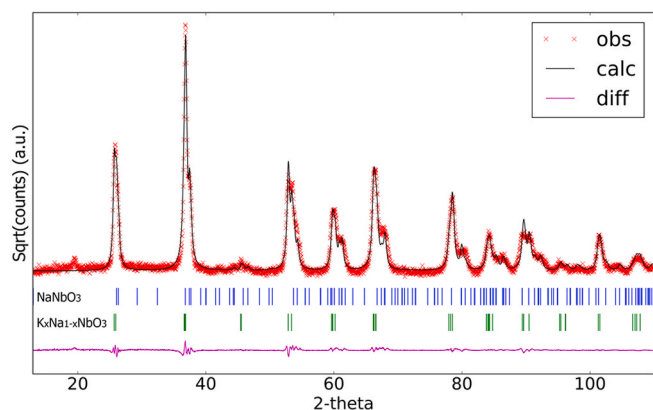
Fig. 3. Rietveld refinement example of the XRD pattern collected from KNN_8 M_24 h sample. The intensity scale is reported as the square root of integrating counts. Red crosses correspond to the experimental data (**obs**), whereas continuous black line represents the modeled signal (**calc**); below the pattern, reflection marks positions and then the residual error plot (**diff**) are reported. (For interpretation of the references to colour in this figure legend, the reader is referred to the Web version of this article.)

96-101-1065).

The effect of reaction time was analyzed under 8 M total OH^- concentration, and the data is given in Fig. 2(b). At the third hour of the reaction, there was still unreacted NbO_2 in addition to the mixed hexaniobate phase ($K_xNa_{8-x}Nb_6O_{19}$. nH_2O) which was already reported as KNN-hydrate in the literature as the intermediate phase during the KNN synthesis [26–30]. Plausibly, NbO_2 dissolves into $Nb_6O_{19}^{8-}$ (Lindqvist ion) in such an alkaline environment following the reaction path (**I**) in a similar fashion with Nb_2O_5 as demonstrated previously by path (**II**) [26, 29,31].

$$6NbO_2 + 14OH^- \rightarrow Nb_6O_{19}^{8-} + 7H_2O \qquad (I)$$

$$3Nb_2O_5 + 8OH^- \rightarrow Nb_6O_{19}^{8-} + 4H_2O \qquad (II)$$

After 6 h of reaction time, both perovskite $K_xNa_{1-x}NbO_3$ and secondary $NaNbO_3$ phases were observed, similar to the observations of Handoko and Goh [28]. It is important to mention that Gibbs free energies of formation for $KNbO_3$ and $NaNbO_3$ were reported as -49 J mol^{-1} and -59 J mol^{-1}, respectively, indicating that $NaNbO_3$ formation is thermodynamically more favorable than that of $KNbO_3$ under identical conditions [32].

Quantitative powder diffraction analysis was performed by full-profile Rietveld approach as implemented in the software ReX [33], by starting from a two-phase sample model containing $K_xNa_{1-x}NbO_3$ and $NaNbO_3$. Reference crystal structures for both phases were obtained from Ref. [34]; both compounds crystallize in the orthorhombic crystal system for the considered conditions, with $K_xNa_{1-x}NbO_3$ in the *Amm*2 space group and $NaNbO_3$ in the $P2_1ma$ space group. The optimization procedure was performed in multiple steps, progressively enabling refinable parameters from the most to the least stable. In the first run, only polynomial background parameters and phase scale factors were

enabled; then, orthorhombic lattice parameters of $K_xNa_{1-x}NbO_3$ phase were added. $NaNbO_3$ lattice parameters were not refined, as this crystal structure is expected to remain relatively stable. In the final step, the most critical parameters were refined, namely the (1-x) occupancy factor of Na element in the K_1 site of $K_xNa_{1-x}NbO_3$ (located at 0.5, 0.0, 0.5209) and the average crystalline domain size, which was set equal for both phases. The latter approximation was introduced to avoid instabilities in the refinement, especially for low-$NaNbO_3$ content samples, and can potentially decrease phase quantification accuracy; however, it should have no effect on $K_xNa_{1-x}NbO_3$ cell parameters and occupancy factors quantification. Fig. 3 reports an example Rietveld refinement for sample KNN_8 M_24 h, clearly showing the presence of both $K_xNa_{1-x}NbO_3$ and $NaNbO_3$ crystallographic phases and a good agreement between experimental and modeled data.

Table 1 reports quantitative results as obtained from Rietveld refinement, in particular $NaNbO_3$ and $K_xNa_{1-x}NbO_3$ volume fractions, $K_xNa_{1-x}NbO_3$ lattice parameters and Na statistical occupancy of the K1 site for the same phase. Parameter errors estimated from the least-squares algorithm are reported as standard deviations on the last significant digit. R_{wp} fitness values show a good agreement between experimental data and the calculated model. Although all the considered samples exhibit the presence of secondary $NaNbO_3$ phase in variable amounts, the lowest amount being 3.74 %vol was observed from the sample processed under 10 M for 24 h (KNN_10 M_24 h). It is possible to state that the amount of potassium incorporated in the lattice increased as the alkalinity increased, such that, $K_{0.99}Na_{0.01}NbO_3$ was formed for 10 M alkaline concentration solution. When alkalinity was fixed constant, upon 6, 12, and 24 h reactions, $K_{0.84}Na_{0.16}NbO_3$, $K_{0.85}Na_{0.15}NbO_3$ and $K_{0.87}Na_{0.13}NbO_3$ were formed, respectively. In other words, slightly further potassium was found to accumulate in the lattice as the reaction time was enhanced.

In this work, only K-rich KNN powders were able to be synthesized, and thus in the additional experiments, the selected sample which was initially composed of 14.34 vol% $NaNbO_3$ and 85.66 vol% $K_{0.84}Na_{0.16}NbO_3$ (8 M_6 h, see Table 1) was post-heat treated at 800 °C for 2 h dwell time (in air). The XRD analysis followed by the Rietveld refinement revealed that the stoichiometry of the annealed sample became $K_{0.61}Na_{0.39}NbO_3$ (sample 8 M_6 h_HT in Table 1). Increased sodium occupancy (from 0.16 to 0.39) indicates that such process facilitates sodium incorporation within the KNN lattice, akin to the observations in the relevant works [28,35].

It is worth emphasizing that typically the structural characterization of KNN powders by XRD is done by matching it with the reference ICDD database pattern of $KNbO_3$ [14,36]. However, despite being isostructural, there is small but critical shift between the patterns of those two phases as can be seen at the bottom of Fig. 2(a). Such shift makes the structural characterization of KNN, especially the stoichiometry, challenging without at least one of the further methods such as Rietveld refinement [28,30], Inductively Coupled Plasma (ICP) spectroscopy [37], Energy Dispersive X-ray analysis (EDX) [37–40] or X-ray fluorescence (XRF) spectrometer [26,41,42].

SEM images of the samples synthesized at 3 h, 6 h, and 12 h are given in Fig. 4(a–c). Dodecahedra-shaped [28] hexaniobate particles can be seen in Fig. 4(a) as corroborated by XRD analyses. After 6 h of reaction (Fig. 4(b)), cube-like morphology of perovskite $K_xNa_{1-x}NbO_3$ agreeing

Table 1
Quantitative parameters obtained from Rietveld refinements.

| Sample	R_{wp}	NaNbO$_3$, phase (% vol)	K$_x$Na$_{1-x}$NbO$_3$ phase (% vol)	K$_x$Na$_{1-x}$NbO$_3$ cell a (Å)	K$_x$Na$_{1-x}$NbO$_3$ cell b (Å)	K$_x$Na$_{1-x}$NbO$_3$ cell c (Å)	Na occupancy, (1-x)
6 M_24 h	0.1416	28.17(2)	71.83(2)	3.98103(2)	5.67883(4)	5.69367(4)	0.1620(9)
8 M_6 h	0.1410	14.34(2)	85.66(3)	3.98120(2)	5.68333(6)	5.68208(6)	0.1635(8)
8 M_12 h	0.1363	18.01(2)	81.99(3)	3.98295(2)	5.69063(10)	5.6804(1)	0.1545(9)
8 M_24 h	0.1399	15.57(2)	84.43(3)	3.97979(2)	5.67991(5)	5.68700(5)	0.1334(9)
10 M_24 h	0.1515	3.74(1)	96.26(3)	3.97521(2)	5.67971(6)	5.70435(6)	0.013(1)
8 M_6 h_HT	0.1118	–	100	3.95011(2)	5.67618(3)	5.64923(3)	0.3847(10)
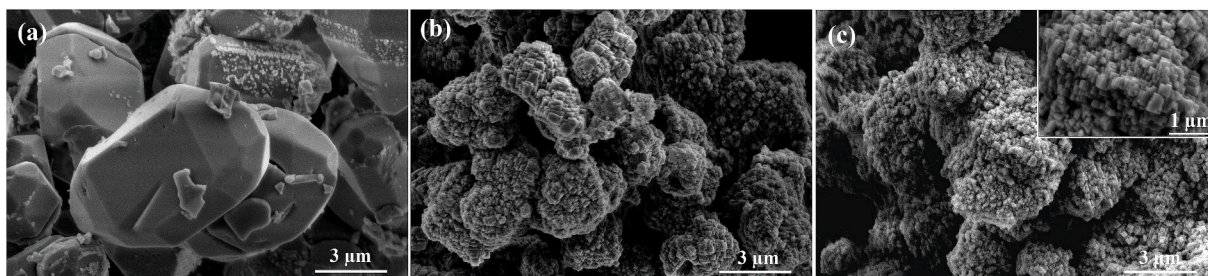
Fig. 4. SEM images of KNN powders synthesized at 200 °C by reacting the alkaline solution of total 8 M total OH⁻ concentration with NbO₂; **(a)** 3 h, **(b)** 6 h, **(c)** 12 h, the inset shows surface detail of the same sample from higher magnification.
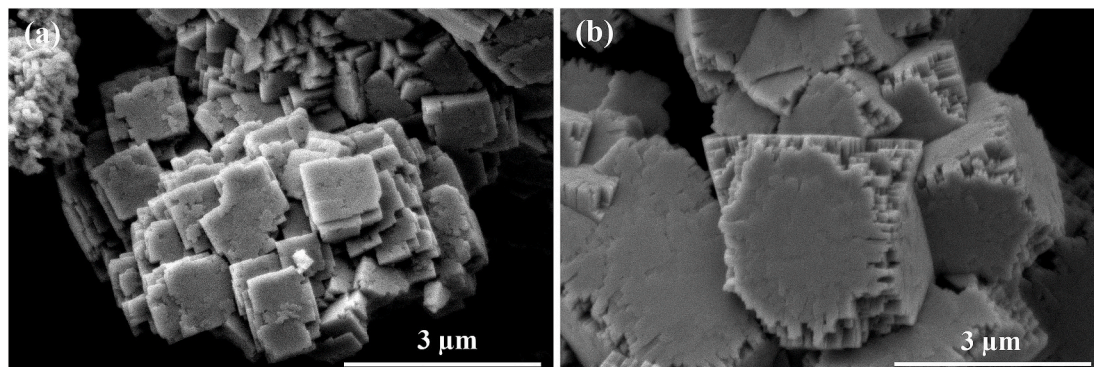

Fig. 5. SEM images of KNN powders synthesized at 200 °C by reacting the alkaline solution with NbO₂ for 24 h under; **(a)** 8 M, **(b)** 10 M.

well with the reported results was observed [17,28,35]. The morphological alteration seen from Fig. 4(a)–4(c) implies that the intermediate hexaniobate phase was replaced by the smaller cube-like KNN crystals (see the inset given in Fig. 4(c)), probably via the dissolution-reprecipitation mechanism as proposed in other KNN synthesis studies [26,28], forming eventually irregularly shaped aggregates.

The morphology for the sample synthesized at the end of the 24 h reaction under 8 M alkalinity is given in Fig. 5(a). As the reaction proceeds, the morphology observed for the 12 h reaction shown in Fig. 4(c) started to disappear while transforming into 1 μm sized cube-like structures as seen in Fig. 5(a). When the alkalinity level was increased to 10 M for the identical reaction period, larger crystals reaching approximately 3 μm in size were noted, see Fig. 5(b). Penn and Banfield [43] proposed an *oriented attachment* concept in which large particles are formed by coalescence of oriented primary particles. Apparently, the concept operates for KNN as well [26,35], and the irregularly shaped KNN aggregates grow via the oriented attachment under 10 M alkaline solution to form the cube shaped crystals.

4. Conclusions

$K_xNa_{1-x}NbO_3$ ($0 < x < 1$) ceramic powders were synthesized by following hydrothermal reaction route with altered alkaline concentration and reaction time. For the first time, niobium dioxide (NbO_2), a metastable niobium oxide phase was used as the niobium source for KNN synthesis. K-rich $K_xNa_{1-x}NbO_3$ ($x > 0.5$) phases were obtained at 200 °C in 6 h by reacting the NbO_2 with KOH/NaOH under 8 M total hydroxide concentration. While the increase in both reaction time and alkalinity level, led to further incorporation of potassium ions, the impact of the latter was more effective and resulted in higher K-rich $K_xNa_{1-x}NbO_3$ ($x > 0.8$) phases. Around 3 μm in sized cube shaped crystals were observed under 10 M reaction in 24 h time reaction.

Declaration of competing interest

The authors declare that they have no known competing financial interests or personal relationships that could have appeared to influence the work reported in this paper.

References

[1] K. Uchino, The Development of Piezoelectric Materials and the New Perspective, Advanced Piezoelectric Materials (2017) 1–92. Elsevier.

[2] T. Zheng, J. Wu, D. Xiao, J. Zhu, Recent development in lead-free perovskite piezoelectric bulk materials, Prog. Mater. Sci. 98 (2018) 552–624, https://doi.org/10.1016/j.pmatsci.2018.06.002.

[3] G.H. Haertling, Ferroelectric ceramics: history and technology, J. Am. Ceram. Soc. 82 (4) (1999) 797–818, https://doi.org/10.1111/j.1151-2916.1999.tb01840.x.

[4] N.M. Hagh, B. Jadidian, A. Safari, Property-processing relationship in lead-free (K, Na, Li) NbO₃ - solid solution system, J. Electroceram. 18 (3–4) (2007) 339–346, https://doi.org/10.1007/s10832-007-9171-x.

[5] J.F. Li, K. Wang, F.Y. Zhu, L.Q. Cheng, F.Z. Yao, (K, Na) NbO₃-based lead-free piezoceramics: fundamental aspects, processing technologies, and remaining challenges, J. Am. Ceram. Soc. 96 (12) (2013) 3677–3696, https://doi.org/10.1111/jace.12715.

[6] E.W.R. Directive, 19/EU of the European Parliament and of the Council of on Waste Electrical and Electronic Equipment (WEEE), Off, J. Eur. Union 197 (2003) 38–71.

[7] E. Directive, I. RoHS, Restriction of the Use of Certain Hazardous Substances in Electrical and Electronic Equipment, European Union, Brussels, Belgium, 2010. Report (A7-0196).

[8] J. Rödel, W. Jo, K.T. Seifert, E.M. Anton, T. Granzow, D. Damjanovic, Perspective on the development of lead-free piezoceramics, J. Am. Ceram. Soc. 92 (6) (2009) 1153–1177, https://doi.org/10.1111/j.1551-2916.2009.03061.x.

[9] J. Wu, D. Xiao, J. Zhu, Potassium–sodium niobate lead-free piezoelectric materials: past, present, and future of phase boundaries, Chem. Rev. 115 (7) (2015) 2559–2595, https://doi.org/10.1021/cr5006809.

[10] M. Kosec, B. Malič, A. Benčan, T. Rojac, KNN-based Piezoelectric Ceramics, Piezoelectric and Acoustic Materials for Transducer Applications, Springer (2008) 81–102.

[11] L. Egerton, D.M. Dillon, Piezoelectric and dielectric properties of ceramics in the system potassium—sodium niobate, J. Am. Ceram. Soc. 42 (9) (1959) 438–442, https://doi.org/10.1111/j.1151-2916.1959.tb12971.x.

[12] Y.-J. Dai, X.-W. Zhang, K.-P. Chen, Morphotropic phase boundary and electrical properties of $K_{1-x}Na_xNbO_3$ lead-free ceramics, Appl. Phys. Lett. 94 (4) (2009), 042905, https://doi.org/10.1063/1.3076105.

[13] B.P. Zhang, J.F. Li, K. Wang, H. Zhang, Compositional dependence of piezoelectric properties in $Na_xK_{1-x}NbO_3$ lead-free ceramics prepared by spark plasma sintering, J. Am. Ceram. Soc. 89 (5) (2006) 1605–1609, https://doi.org/10.1111/j.1551-2916.2006.00960.x.

[14] M. Kosec, B. Benčan, T. Rojac, J. Tellier, Alkaline niobate-based piezoceramics: crystal structure, synthesis, sintering and microstructure, Funct. Mater. Lett. 3 (1) (2010) 15–18, https://doi.org/10.1142/S1793604710000865.

[15] E. Ringgaard, T. Wurlitzer, Lead-free piezoceramics based on alkali niobates, J. Eur. Ceram. Soc. 25 (12) (2005) 2701–2706, https://doi.org/10.1016/j.jeurceramsoc.2005.03.126.

[16] Y. Wang, D. Damjanovic, N. Klein, N. Setter, High-temperature instability of Li-and Ta-modified (K, Na) NbO_3 piezoceramics, J. Am. Ceram. Soc. 91 (6) (2008) 1962–1970, https://doi.org/10.1111/j.1551-2916.2008.02392.x.

[17] L.A. Ramajo, F. Rubio-Marcos, A. Del Campo, J.F. Fernández, M.S. Castro, R. Parra, New insights into the properties of $K_xNa_{(1-x)}NbO_3$ ceramics obtained by hydrothermal synthesis, Ceram. Int. 40 (9) (2014) 14701–14712, https://doi.org/10.1016/j.ceramint.2014.06.059.

[18] S. Bai, T. Karaki, Two-step synthesis of platelike potassium sodium niobate template particles by hydrothermal method, J. Am. Ceram. Soc. 96 (8) (2013) 2515–2518, https://doi.org/10.1111/jace.12345.

[19] F. Zhang, L. Han, S. Bai, T. Sun, T. Karaki, M. Adachi, Hydrothermal synthesis of (K, Na) NbO_3 particles, Jpn. J. Appl. Phys. 47 (9S) (2008) 7685, https://doi.org/10.1143/JJAP.47.7685.

[20] L. Bai, K. Zhu, L. Su, J. Qiu, H. Ji, Synthesis of (K, Na) NbO_3 particles by high temperature mixing method under hydrothermal conditions, Mater. Lett. 64 (1) (2010) 77–79, https://doi.org/10.1016/j.matlet.2009.10.013.

[21] C. Nico, T. Monteiro, M.P. Graça, Niobium oxides and niobates physical properties: review and prospects, Prog. Mater. Sci. 80 (2016) 1–37, https://doi.org/10.1016/j.pmatsci.2016.02.001.

[22] K. Senevirathne, R. Hui, S. Campbell, S. Ye, J. Zhang, Electrocatalytic activity and durability of Pt/NbO_2 and Pt/Ti_4O_7 nanofibers for PEM fuel cell oxygen reduction reaction, Electrochim. Acta 59 (2012) 538–547, https://doi.org/10.1016/j.electacta.2011.11.005.

[23] L. Kong, C. Zhang, J. Wang, W. Qiao, L. Ling, D. Long, Nanoarchitectured Nb_2O_5 hollow, $Nb_2O_5@carbon$ and $NbO_2@carbon$ core-shell microspheres for ultrahigh-rate intercalation pseudocapacitors, Sci. Rep. 6 (1) (2016) 1–10, https://doi.org/10.1038/srep21177.

[24] P. Biggin, G. Smith, I. Shrivastava, S. Choe, M. Sansom, Potassium and sodium ions in a potassium channel studied by molecular dynamics simulations, Biochim. Biophys. Acta Biomembr. 1510 (1–2) (2001) 1–9, https://doi.org/10.1016/S0005-2736(00)00345-X.

[25] J.H. Lv, M. Zhang, M. Guo, W.C. Li, X.D. Wang, Hydrothermal synthesis and characterization of $K_xNa_{(1-x)}NbO_3$ powders, Int. J. Appl. Ceram. Technol. 4 (6) (2007) 571–577, https://doi.org/10.1111/j.1744-7402.2007.02165.x.

[26] Z. Wang, H. Gu, Y. Hu, K. Yang, M. Hu, D. Zhou, J. Guan, Synthesis, growth mechanism and optical properties of (K, Na) NbO_3 nanostructures, CrystEngComm 12 (10) (2010) 3157–3162, https://doi.org/10.1039/C000169D.

[27] M. Zhang, M. Guo, Y. Zhou, Low-temperature preparation of $K_xNa_{(1-x)}NbO_3$ lead-free piezoelectric powders by microwave-hydrothermal synthesis, Int. J. Appl.

Ceram. Technol. 8 (3) (2011) 591–596, https://doi.org/10.1111/j.1744-7402.2009.02464.x.

[28] A.D. Handoko, G.K. Goh, Hydrothermal synthesis of sodium potassium niobate solid solutions at 200°C, Green Chem. 12 (4) (2010) 680–687, https://doi.org/10.1039/B923840A.

[29] G.K. Goh, F.F. Lange, S.M. Haile, C.G. Levi, Hydrothermal synthesis of $KNbO_3$ and $NaNbO_3$ powders, J. Mater. Res. 18 (2) (2003) 338–345, https://doi.org/10.1557/JMR.2003.0044.

[30] S.L. Skjærvø, K.H. Wells, W. Van Beek, T. Grande, M.-A. Einarsrud, Kinetics during hydrothermal synthesis of nanosized $K_xNa_{1-x}NbO_3$, CrystEngComm 20 (42) (2018) 6795–6802, https://doi.org/10.1039/C8CE01178H.

[31] H. Zhu, Z. Zheng, X. Gao, Y. Huang, Z. Yan, J. Zou, H. Yin, Q. Zou, S.H. Kable, J. Zhao, Structural evolution in a hydrothermal reaction between Nb_2O_5 and NaOH solution: from Nb_2O_5 grains to microporous $Na_2Nb_2O_6.2/3H_2O$ fibers and $NaNbO_3$ cubes, J. Am. Ceram. Soc. 128 (7) (2006) 2373–2384, https://doi.org/10.1021/ja056301w.

[32] C. Zhang, L. Haijun, G. Min, M. Zhang, W. Xidong, Thermodynamic evaluation and hydrothermal preparation of $K_xNa_{1-x}NbO_3$, Rare Met. 27 (4) (2008) 371–377, https://doi.org/10.1016/S1001-0521(08)60148-5.

[33] M. Bortolotti, L. Lutterotti, I. Lonardelli, ReX: a computer program for structural analysis using powder diffraction data, J. Appl. Crystallogr. 42 (3) (2009) 538–539, https://doi.org/10.1107/S0021889809008309.

[34] M. Ahtee, A. Hewat, Structural phase transitions in sodium-potassium niobate solid solutions by neutron powder diffraction, Acta Crystallogr. A 34 (2) (1978) 309–317, https://doi.org/10.1107/S056773947800056X.

[35] G. Shi, J. Wang, H. Wang, Z. Wu, H. Wu, Hydrothermal synthesis of morphology-controlled $KNbO_3$, $NaNbO_3$, and (K, Na) NbO_3 powders, Ceram. Int. 43 (9) (2017) 7222–7230, https://doi.org/10.1016/j.ceramint.2017.03.012.

[36] A.B. Haugen, F. Madaro, L.-P. Bjørkeng, T. Grande, M.-A. Einarsrud, Sintering of sub-micron $K_{0.5}Na_{0.5}NbO_3$ powders fabricated by spray pyrolysis, J. Eur. Ceram. Soc. 35 (5) (2015) 1449–1457, https://doi.org/10.1016/j.jeurceramsoc.2014.11.011.

[37] S. Xu, J.F. Li, Synthesis and piezoelectricity of single-crystalline (K, Na) NbO_3 nanobars, J. Am. Ceram. Soc. 94 (11) (2011) 3812–3818, https://doi.org/10.1111/j.1551-2916.2011.04722.x.

[38] D. Zhang, F. Shi, J. Cheng, Z. Cheng, X. Yang, G. Zheng, M. Cao, Modified hydrothermal synthesis and structural characterization of monoclinic $(K_xNa_{1-x})NbO_3$ $(0.05 \leq x \leq 0.15)$ rods, Ceram. Int. 41 (7) (2015) 8837–8842, https://doi.org/10.1016/j.ceramint.2015.03.113.

[39] H. Xu, M.-R. Joung, J.-S. Kim, S. Nahm, M.-G. Kang, C.-Y. Kang, S.-J. Yoon, Synthesis of homogeneous $(Na_{1-x}K_x)$ NbO3 nanorods using hydrothermal and post-heat treatment processes, Chem. Eng. J. 211 (2012) 16–21, https://doi.org/10.1016/j.cej.2012.09.052.

[40] R. López-Juárez, O. Novelo-Peralta, F. González-García, F. Rubio-Marcos, M.-E. Villafuerte-Castrejón, Ferroelectric domain structure of lead-free potassium-sodium niobate ceramics, J. Eur. Ceram. Soc. 31 (9) (2011) 1861–1864, https://doi.org/10.1016/j.jeurceramsoc.2011.02.031.

[41] M. Zheng, Y. Hou, L. Chao, M. Zhu, Piezoelectric KNN ceramic for energy harvesting from mechanochemically activated precursors, J. Mater. Sci. Mater. Electron. 29 (11) (2018) 9582–9587, https://doi.org/10.1007/s10854-018-8993-4.

[42] H. Ge, Y. Hou, J. Yang, M. Zhu, H. Wang, H. Yan, Fabrication and properties of $Na_{0.9}K_{0.1}NbO_3$ nanostructures by molten salt synthesis, Powder Technol. 246 (2013) 144–147, https://doi.org/10.1016/j.powtec.2013.05.013.

[43] R.L. Penn, J.F. Banfield, Morphology development and crystal growth in nanocrystalline aggregates under hydrothermal conditions: insights from titania, Geochem. Cosmochim. Acta 63 (10) (1999) 1549–1557, https://doi.org/10.1016/S0016-7037(99)00037-X.